

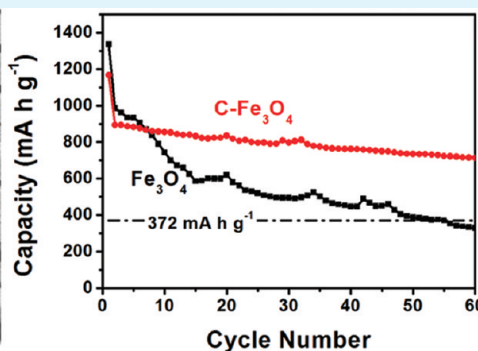
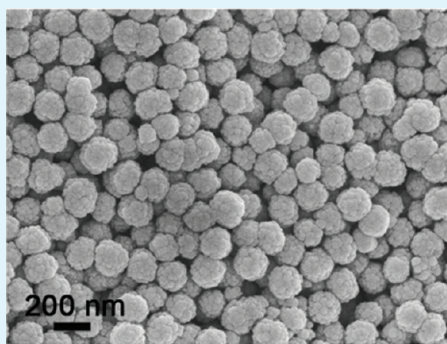
One-Pot Synthesis of Uniform Fe₃O₄ Nanospheres with Carbon Matrix Support for Improved Lithium Storage Capabilities

Jun Song Chen,^{†,‡,§} Yumiao Zhang,^{†,§} and Xiong Wen (David) Lou^{*,†,‡}

[†]School of Chemical and Biomedical Engineering, Nanyang Technological University, 70 Nanyang Drive, Singapore 637457

[‡]Energy Research Institute @ NTU, Nanyang Technological University, 50 Nanyang Drive, Singapore 637553

ABSTRACT:

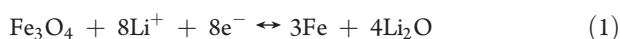


Poly(acrylic acid) (PAA)-entangled Fe₃O₄ nanospheres are synthesized via a facile solvothermal method. In this system, ethylenediamine plays a very important role to control the uniformity of the nanospheres, and the PAA molecules serve as the carbon source that transforms into a carbon matrix after the heat treatment under an inert atmosphere. These uniform Fe₃O₄ nanospheres with carbon matrix support manifest greatly enhanced lithium storage properties over prolonged cycling, with a reversible capacity of 712 mA h g⁻¹ retained after 60 charge/discharge cycles. However, the carbon-free counterpart can only deliver a much lower capacity of 328 mA h g⁻¹.

KEYWORDS: Fe₃O₄, carbon matrix, lithium-ion batteries, anode

INTRODUCTION

Magnetite (Fe₃O₄) has been a widely studied material. Because of its electroactivity, and biocompatibility,¹ Fe₃O₄ has attracted enormous research interests in lithium storage,^{2–9} targeted drug delivery,^{10–12} and water treatment.¹³ Because of the unique magnetic nature of Fe₃O₄,^{14–19} it has also been applied in magnetism,^{20–24} as well as magnetic resonance imaging.^{25–27} When serving as the anode material for lithium-ion batteries, the following equation summarizes the electrochemical reaction between Fe₃O₄ and Li



This shows that Fe₃O₄ has a theoretical capacity of ~900 mA h g⁻¹, which is much higher than that of the commercially used graphite (~372 mA h g⁻¹). However, as a transition metal oxide, Fe₃O₄ has the intrinsic drawback of low electronic conductivity. Furthermore, many side reactions during the charge/discharge process, such as the formation of solid-electrolyte interface (SEI) films on the electrode surface, will cause extra consumption of Li, leading to large initial irreversible capacity loss.

It is believed that carbon nanocoating is an effective surface modification method to improve the performance of the electrode materials.⁵ The coated carbon layer can buffer the volume change during the charge/discharge process because of its elastic

nature. Additionally, it can also improve the electronic conductivity of the composite. To date, carbon coating usually requires an additional step to deposit a layer of amorphous carbon on the surface of the pre-synthesized electroactive material,⁵ which complicates the synthesis scheme. It is thus more desirable to develop a one-pot facile strategy to introduce the carbon into the composite.^{2,7,28,29}

Herein, we use a one-pot poly(acrylic acid) (PAA)-mediated solvothermal method to synthesize Fe₃O₄ nanospheres. As shown in Figure 1, the PAA molecules not only are the structure coordinating agents that assist in the formation of the spherical structure (step I),^{20,27} but also serve as the carbon source that would be subsequently carbonized to give rise to a carbon matrix (step II). We further show that the addition of a small amount of ethylenediamine (EDA) into the system will lead to the formation of much more uniform Fe₃O₄ nanospheres with narrow size distribution.¹⁷ During the electrochemical measurement, the carbon matrix-supported Fe₃O₄ nanospheres (C-Fe₃O₄) demonstrate much better lithium storage properties than the carbon-free counterpart, with a high reversible capacity of 712 mA h g⁻¹ after 60 charge/discharge cycles.

Received: August 12, 2011

Accepted: September 9, 2011

Published: September 09, 2011

EXPERIMENTAL SECTION

Materials Synthesis. The C-Fe₃O₄ nanospheres were synthesized via a modified solvothermal method.²⁷ Briefly, 1.5 g sodium acetate (NaAc), 1.5 g sodium acrylate (CH₂=CHCOONa, Na acrylate) and 0.54 g Ferric chloride hexahydrate (FeCl₃·6H₂O) were slowly dissolved in 19 ml of ethylene glycol (EG) to obtain a homogenous solution. In order to improve the uniformity of the Fe₃O₄ nanospheres, 1–2 mL of ethylenediamine (EDA) was added. Then, the resulting yellow solution was transferred into a 40 ml Teflon-lined stainless steel autoclave and kept at 200 °C for 12 h. After cooling down to room temperature, the



Figure 1. Schematic illustration of the formation of the carbon matrix-supported uniform Fe₃O₄ nanospheres. I: formation of the PAA-entangled Fe₃O₄ nanospheres. II: carbonization of PAA into carbon matrix.

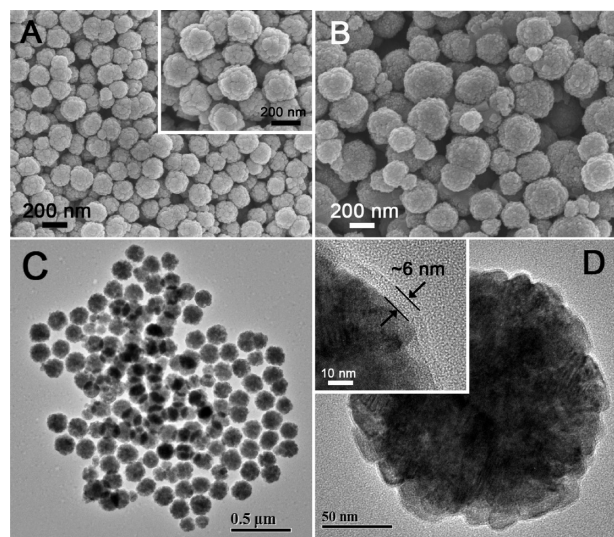


Figure 2. SEM images of the Fe₃O₄ nanospheres synthesized (A) with and (B) without the addition of EDA. The inset in A shows a high-magnification SEM image of the sample. (C, D) TEM images of the PAA-entangled Fe₃O₄ nanospheres after carbonization. The inset in D is a magnified image showing the carbon layer.

precipitate was harvested by centrifugation and washed with water and ethanol. Subsequently, the products were dried in 60 °C overnight. In order to get C-Fe₃O₄, the as-synthesized PAA-entangled nanospheres were heated in N₂ for 6 h at 500 °C with a heating rate of 5 °C min⁻¹.

Material Characterizations. The morphology of products was examined by transmission electron microscope (TEM; JEOL, JEM-2100F, 200 kV, with electron diffraction), field-emission scanning electron microscope (FESEM; JEOL, JSM-6700F, 5 kV). Crystallographic information of the samples was investigated with X-ray powder diffraction (XRD; Bruker, D8 - Advance X-ray Diffractometer, Cu Kα, λ = 1.5406 Å). Thermogravimetric analysis (TGA) was carried out under a flow of air with a temperature ramp of 5 °C min⁻¹. The nitrogen adsorption was performed using a Quantachrome Instrument (Autosorb AS-6B).

Electrochemical Measurements. The electrochemical measurements were carried out using two-electrode Swagelok cells (X2 Lab-ware, Singapore) with pure lithium metal as both the counter and the reference electrodes at room temperature. The working electrode consisted of active material (e.g., C-Fe₃O₄ nanospheres), a conductive agent (carbon black, Super-P-Li), and a polymer binder (poly(vinylidene difluoride), PVDF, Aldrich) in a 70:20:10 weight ratio. The electrolyte used was 1.0 M LiPF₆ in a 50:50 (w/w) mixture of ethylene carbonate and diethyl carbonate. Cell assembly was carried out in an Ar-filled glovebox with concentrations of moisture and oxygen below 1.0 ppm. Cyclic voltammetry (0.01–3 V, 0.5 mV s⁻¹) was performed using an electrochemical workstation (CHI 660C). The charge/discharge tests were performed using a NEWARE battery tester at different current rates with a voltage window of 0.05–2.5 V at a current rate of 200 mA g⁻¹.

RESULTS AND DISCUSSION

Figure 2A shows the scanning electron microscopy (SEM) image of the as-prepared C-Fe₃O₄ nanospheres. It is very clear that the sample contains very uniform spherical particles with a diameter ranging from 150 to 200 nm. Under higher magnification (Figure 2A, inset), the nanospheres are shown to be composed of small irregular particles, and have a relatively rough surface. In the control experiment where no EDA is added, the obtained particles are much less uniform (Figure 2B), with a wider size distribution of 100–500 nm. We thus hypothesize that EDA may act like a surfactant which further controls the crystal growth of the Fe₃O₄ nanoparticles during nucleation, allowing the formation of nanospheres with smaller size. The uniform spherical structure is confirmed under transmission electron microscopy (TEM), with the images shown in Figure 2C. Figure 2D depicts a single C-Fe₃O₄ nanosphere, and the inset demonstrates that the sphere is actually coated with a thin layer of amorphous carbon with a uniform thickness of ~6 nm. Such a structure possesses a specific surface area of ~29 m² g⁻¹.

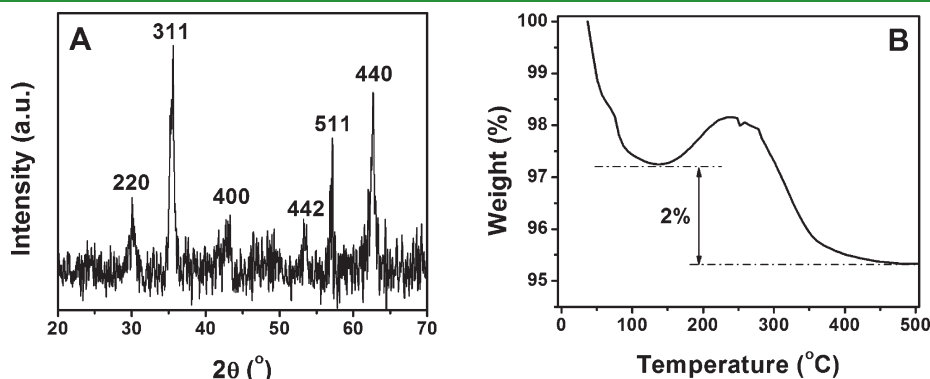


Figure 3. (A) XRD pattern and (B) TGA data of the as-prepared C-Fe₃O₄ nanospheres.

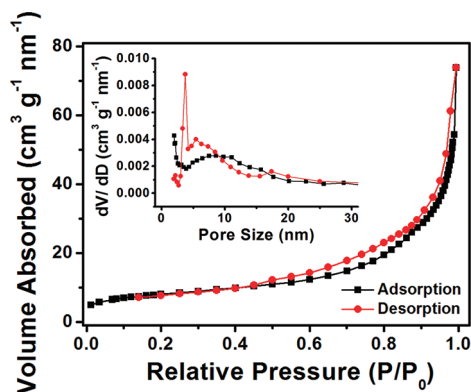


Figure 4. N_2 adsorption–desorption isotherm of the PAA-entangled Fe_3O_4 nanospheres after carbonization. The inset shows the pore size distributions from both branches.

The chemical composition of the sample is determined by X-ray diffraction (XRD), with the result shown in Figure 3A. All the identified peaks can be perfectly assigned to face-centered-cubic magnetite Fe_3O_4 (JCPDS card No. 19-0629, S.G.: $Fd\bar{3}m$, $a_0 = 8.396 \text{ \AA}$). The relatively low intensity of the diffraction peaks indicates the formation of small-size nanograins in each of the nanospheres. The carbon content is determined by thermogravimetric analysis (TGA; Figure 3B). It can be noticed that the weight loss below $150 \text{ }^\circ\text{C}$ could be probably attributed to the evaporation of the adsorbed moisture or gaseous molecules,⁷ and the major weight loss takes place at $\sim 350 \text{ }^\circ\text{C}$ and completes at $\sim 500 \text{ }^\circ\text{C}$, giving rise to an observed weight loss of $\sim 2\%$. While considering that Fe_3O_4 will be converted into Fe_2O_3 when heated in air, it will cause a weight increase of about $\sim 3.45\%$.³⁰ Thus, the actual carbon content in the C- Fe_3O_4 sample can then be estimated to be $\sim 5.45\%$. Figure 4 shows the N_2 adsorption-desorption isotherm of the sample. It might be categorized as type III isotherm without a distinct hysteresis loop. This is quite conceivable, as the transformation of the PAA polymer into carbon will probably lead to certain structural alteration, which might block the pores and make them inaccessible. As a result, a relatively low surface area of $\sim 30 \text{ m}^2 \text{ g}^{-1}$ is observed. The pore size distribution reveals that the sample possesses pores with a diameter less than 10 nm .

We subsequently evaluated the lithium storage properties of the as-prepared C- Fe_3O_4 nanospheres. Figure 5A shows the representative cyclic voltammograms (CVs) for the first two cycles, between 0.01 and 3 V with a scan rate of 0.5 mV s^{-1} . It exhibits a pattern that is consistent with the previously reported data.⁷ A dominant pair of redox peaks can be clearly identified in the first cycle at ~ 0.4 and $\sim 2.0 \text{ V}$, during the cathodic and anodic sweep, respectively. The current intensity of the cathodic peak reduces noticeably in the second cycle, accompanied by a slight shift of its voltage position, indicating the occurrence of irreversible processes in the electrode material. However, there is no obvious change in the anodic peak, suggesting that the electrochemical reaction has proceeded to a similar extent.

Figure 5B depicts the charge/discharge voltage profiles for the first, second, and fifth cycles. The sample shows a very high first-cycle discharge capacity of 1166 mA h g^{-1} , which is even higher than the theoretical capacity of Fe_3O_4 . This could be probably due to the formation of the SEI film. It delivers a corresponding charge capacity of 893 mA h g^{-1} , giving rise to an irreversible

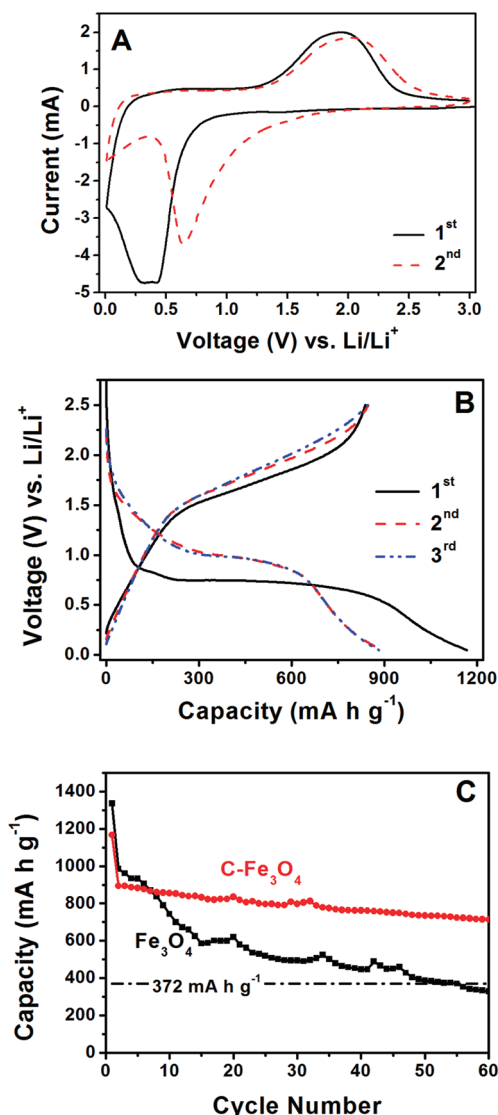


Figure 5. (A) Representative cyclic voltammograms, (B) charge–discharge voltage profiles of the as-prepared C- Fe_3O_4 nanospheres, and (C) comparative cycling performance of the C- Fe_3O_4 and pure Fe_3O_4 nanospheres.

capacity loss of $\sim 23\%$. The Coulombic efficiency quickly increases to 95 and 96% in the second and fifth cycle, respectively. The comparative cycling performance between the C- Fe_3O_4 and carbon-free Fe_3O_4 nanospheres is illustrated in Figure 5C. Apparently, the sample with carbon matrix support demonstrates a much better cyclic retention than the carbon-free one, with a high reversible capacity of 712 mA h g^{-1} after 60 cycles, which is much higher than the theoretical capacity of graphite (372 mA h g^{-1}). The pure Fe_3O_4 nanospheres shows a higher initial discharge capacity of $\sim 1337 \text{ mA h g}^{-1}$ than the sample of C- Fe_3O_4 , probably because the C- Fe_3O_4 composite contains a high weight fraction of the inactive amorphous carbon. However, its capacity fades very rapidly during the course of the first few cycles. Compared to the C- Fe_3O_4 sample, a much lower capacity of only 328 is delivered at the end of the 60 cycles. This evidently proves that the positive effect of the carbon matrix support generated by carbonization of the PAA molecules.

CONCLUSION

In this work, we have developed a one-pot solvothermal PAA-mediated method to synthesize Fe₃O₄ nanospheres with carbon matrix support. The PAA molecules serve both as the coordinating agent and the carbon source. Furthermore, it is found that the addition of EDA into the system will significantly improve the uniformity of the Fe₃O₄ nanospheres, giving rise to products with a narrow size distribution. The electrochemical analysis suggests that the carbon-supported sample exhibits a much better cycling performance compared to the carbon-free counterpart, with a high reversible capacity of 712 mA h g⁻¹ after 60 charge/discharge cycles. This shows that the C-Fe₃O₄ products generated by the current technique could become a promising candidate for high-performance lithium-ion batteries.

AUTHOR INFORMATION

Corresponding Author

*E-mail: xwlou@ntu.edu.sg. Tel.: +65 6316 8879; Fax: +65 6791 1761.

Author Contributions

[§]These authors contributed equally.

REFERENCES

- (1) Liu, J.; Sun, Z. K.; Deng, Y. H.; Zou, Y.; Li, C. Y.; Guo, X. H.; Xiong, L. Q.; Gao, Y.; Li, F. Y.; Zhao, D. Y. *Angew. Chem. Int. Ed.* **2009**, *48*, 5875.
- (2) Chen, J. S.; Liu, H.; Qiao, S. Z.; Lou, X. W. *J. Mater. Chem.* **2011**, *21*, 5687.
- (3) Taberna, L.; Mitra, S.; Poizot, P.; Simon, P.; Tarascon, J. M. *Nat. Mater.* **2006**, *5*, 567.
- (4) Wang, J.-Z.; Zhong, C.; Wexler, D.; Idris, N. H.; Wang, Z.-X.; Chen, L.-Q.; Liu, H.-K. *Chem.—Eur. J.* **2011**, *17*, 661.
- (5) Zhang, W. M.; Wu, X. L.; Hu, J. S.; Guo, Y. G.; Wan, L. J. *Adv. Funct. Mater.* **2008**, *18*, 3941.
- (6) Zhou, G.; Wang, D.-W.; Li, F.; Zhang, L.; Li, N.; Wu, Z.-S.; Wen, L.; Lu, G. Q.; Cheng, H.-M. *Chem. Mater.* **2010**, *22*, 5306.
- (7) Zhu, T.; Chen, J. S.; Lou, X. W. *J. Phys. Chem. C* **2011**, *115*, 9814.
- (8) Ban, C. M.; Wu, Z. C.; Gillaspie, D. T.; Chen, L.; Yan, Y. F.; Blackburn, J. L.; Dillon, A. C. *Adv. Mater.* **2010**, *22*, E145.
- (9) Kang, E.; Jung, Y. S.; Cavanagh, A. S.; Kim, G. H.; George, S. M.; Dillon, A. C.; Kim, J. K.; Lee, J. *Adv. Funct. Mater.* **2011**, *21*, 2430.
- (10) Chen, F. H.; Zhang, L. M.; Chen, Q. T.; Zhang, Y.; Zhang, Z. J. *Chem. Commun.* **2010**, *46*, 8633.
- (11) Yang, X. Y.; Zhang, X. Y.; Ma, Y. F.; Huang, Y.; Wang, Y. S.; Chen, Y. S. *J. Mater. Chem.* **2009**, *19*, 2710.
- (12) Zhu, Y. F.; Ikoma, T.; Hanagata, N.; Kaskel, S. *Small* **2010**, *6*, 471.
- (13) Zhong, L. S.; Hu, J. S.; Liang, H. P.; Cao, A. M.; Song, W. G.; Wan, L. J. *Adv. Mater.* **2006**, *18*, 2426.
- (14) He, H.; Gao, C. *ACS Appl. Mater. Interfaces* **2010**, *2*, 3201.
- (15) Wang, H.; Chen, Q. W.; Yu, Y. F.; Cheng, K.; Sun, Y. B. *J. Phys. Chem. C* **2011**, *115*, 11427.
- (16) Deng, Y.; Qi, D.; Deng, C.; Zhang, X.; Zhao, D. *J. Am. Chem. Soc.* **2007**, *130*, 28.
- (17) Li, S. K.; Huang, F. Z.; Wang, Y.; Shen, Y. H.; Qiu, L. G.; Xie, A. J.; Xu, S. J. *J. Mater. Chem.* **2011**, *21*, 7459.
- (18) Liu, Y.; Ren, Z. Y.; Wei, Y. L.; Jiang, B. J.; Feng, S. S.; Zhang, L. Y.; Zhang, W. B.; Fu, H. G. *J. Mater. Chem.* **2010**, *20*, 4802.
- (19) Ye, M. M.; Zhang, Q.; Hu, Y. X.; Ge, J. P.; Lu, Z. D.; He, L.; Chen, Z. L.; Yin, Y. D. *Chem.—Eur. J.* **2010**, *16*, 6243.
- (20) Ge, J. P.; Hu, Y. X.; Biasini, M.; Beyermann, W. P.; Yin, Y. D. *Angew. Chem. Int. Ed.* **2007**, *46*, 4342.
- (21) Jia, C. J.; Sun, L. D.; Luo, F.; Han, X. D.; Heyderman, L. J.; Yan, Z. G.; Yan, C. H.; Zheng, K.; Zhang, Z.; Takano, M.; Hayashi, N.; Eltschka, M.; Klau, M.; Rudiger, U.; Kasama, T.; Cervera-Gontard, L.; Dunin-Borkowski, R. E.; Tzvetkov, G.; Raabe, J. *J. Am. Chem. Soc.* **2008**, *130*, 16968.
- (22) Wang, Y.; Zhu, Q.; Tao, L. *CrystEngComm* **2011**, *13*, 4652.
- (23) Yu, X. G.; Wan, J. Q.; Shan, Y.; Chen, K. Z.; Han, X. D. *Chem. Mater.* **2009**, *21*, 4892.
- (24) Zhang, L.; Qiao, S. Z.; Jin, Y. G.; Chen, Z. G.; Gu, H. C.; Lu, G. Q. *Adv. Mater.* **2008**, *20*, 805.
- (25) Chen, Y.; Chen, H.; Zeng, D.; Tian, Y.; Chen, F.; Feng, J.; Shi, J. *ACS Nano* **2010**, *4*, 6001.
- (26) Lee, J. E.; Lee, N.; Kim, H.; Kim, J.; Choi, S. H.; Kim, J. H.; Kim, T.; Song, I. C.; Park, S. P.; Moon, W. K.; Hyeon, T. *J. Am. Chem. Soc.* **2009**, *132*, 552.
- (27) Xuan, S.; Wang, F.; Lai, J. M. Y.; Sham, K. W. Y.; Wang, Y.-X. J.; Lee, S.-F.; Yu, J. C.; Cheng, C. H. K.; Leung, K. C.-F. *ACS Appl. Mater. Interfaces* **2011**, *3*, 237.
- (28) Liu, J. H.; Chen, J. S.; Wei, X. F.; Lou, X. W.; Liu, X. W. *Adv. Mater.* **2011**, *23*, 998.
- (29) Lou, X. W.; Chen, J. S.; Chen, P.; Archer, L. A. *Chem. Mater.* **2009**, *21*, 2868.
- (30) Deng, H.; Li, X. L.; Peng, Q.; Wang, X.; Chen, J. P.; Li, Y. D. *Angew. Chem., Int. Ed.* **2005**, *44*, 2782.